Characteristics of thunder and electromagnetic pulses from volcanic lightning at Bogoslof Volcano, Alaska

Matthew M. Haney[1]* (0000-0003-3317-7884), Alexa R. Van Eaton[2] (0000-0001-6646-4594), John J. Lyons[1] (0000-0001-5409-1698), Rebecca L. Kramer[2] (0000-0002-4873-1983), David Fee[3] (0000-0002-0936-9977), Alexandra M. Iezzi[3] (0000-0002-6782-7681), Robert P. Dziak[4] (0000-0001-8775-3416), Jacob Anderson[5] (0000-0001-6447-6778), Jeffrey B. Johnson[5] (0000-0003-4179-8592), Jeff L. Lapierre[6] (0000-0002-7176-9808), and Michael Stock[6] ()

[1]U.S. Geological Survey, Alaska Volcano Observatory, Anchorage, AK, USA
[2]U.S. Geological Survey, Cascades Volcano Observatory, Vancouver, WA, USA
[3]Geophysical Institute, University of Alaska Fairbanks, Alaska Volcano Observatory, Fairbanks, AK, USA
[4]NOAA Pacific Marine Environmental Laboratory, Newport, OR, USA
[5]Boise State University, Department of Geosciences, Boise, ID, USA
[6]Earth Networks Inc., Germantown, MD, USA
* Corresponding author: mhaney@usgs.gov

Acknowledgments: The authors wish to thank the World Wide Lightning Location Network (http://wwlln.net), a collaboration among over 50 universities and institutions, for providing lightning location data used in this paper. Thanks to Vaisala (http://www.vaisala.com) for providing lightning location and peak current data. This paper is NOAA-PMEL contribution number ##.

Keywords: Volcano Monitoring, Volcanic Lightning, Explosive Volcanism, Infrasound

Abstract

We combine global detections of volcanic lightning with infrasound and hydroacoustic data to investigate novel indications of plume electrification in ground-based, geophysical data streams during the 2016-17 eruption of Bogoslof Volcano, Alaska. Such signals offer additional ways to diagnose the occurrence of volcanic lightning, and therefore whether eruptive activity is likely producing significant amounts of ash. We discuss three signatures of lightning activity: volcanic thunder, electromagnetic pulses arising from lightning-induced voltages in cabling, and hydroacoustic signals associated with volcanic lightning. Observations of these phenomena provide additional insights into volcanic lightning activity and yield several detections not previously contained in global lightning catalogs.

1. Introduction

Electrification of volcanic plumes is a consequence of grain-scale processes at the volcanic vent that are associated with large, explosive, ash-producing eruptions [Mather and Harrison, 2006]. Although its origins can be traced back to the scale of grains, electrification leads to discharge in the form of lightning that can be measured globally. The ability of worldwide networks of lightning sensors operating in the 3-30 kHz band to detect volcanic lightning has made a baseline of volcanic eruption detection possible, even in remote regions. The drawback of the global networks is that only the most energetic strokes can be detected, which are often classified as plume lightning [Behnke and McNutt, 2014]. Less energetic strokes, especially those close to the vent, and continual radio frequency emissions require local lightning mapping array installations [Thomas et al., 2007]. Detections of volcanic lightning, in addition to their value for monitoring, also offer a window into the dynamics of volcanic plumes [Behnke and Bruning, 2015; Van Eaton et al., 2016].

Recent major eruptions in Alaska have produced detectable volcanic lightning on both local and global lightning sensors, including the 2006 Augustine [Thomas et al., 2007] and 2009 Redoubt [Behnke and McNutt, 2014] eruptions. Bogoslof, a mostly submarine volcano in the Bering Sea, Alaska, produced a prolific amount of volcanic lightning during its eruption sequence from December 2016 to August 2017 [Van Eaton et al., this issue], which was detected globally. Coombs et al. [this issue] provide an overview of the entire eruption sequence. Detections on global lightning networks were used in real-time at the Alaska Volcano Observatory for monitoring the eruption of Bogoslof [Coombs et al., 2018]. In fact, of the 70 explosive events that occurred over the course of the eruption, one event was detected by volcanic lightning only [Coombs et al., 2018].

Although volcanic lightning has received a great deal of attention in recent years, the associated phenomenon of volcanic thunder had not been documented until the Bogoslof eruption [Haney et al., 2018]. This is in contrast to meteorological thunder, which has been studied using combined lightning and infrasound data sets [Assink et al., 2008; Johnson et al., 2011]. The omission for the volcanic case is in large part due to the difficulty of unequivocally identifying thunder signals in acoustic data during eruptive activity, since eruptions themselves radiate intense sound waves due to the ejection of magmatic products at the vent. For the Bogoslof eruption, an array of microphones located 60 km from the volcano allowed precise direction-of-arrival information to be derived from acoustic waves during the eruption. Analysis of the directional information indicated some of the sound waves originated from a different direction than the volcanic vent, thereby implicating thunder as their source [Haney et al., 2018]. Moreover, the distance of the microphone array from the volcano (60 km) placed it within the range where measurements of thunder signals can be expected [Campus and Christie, 2009].

Volcanic thunder turns out to be only one manifestation of volcanic lightning in ground-based geophysical data streams, such as infrasound data. In their study of Tungurahua Volcano in Ecuador, Anderson et al. [2018] highlighted the occurrence of electromagnetic pulses, or glitches, in infrasound data due to volcanic lightning. Similar glitches have been observed in seismic data during the 1992 eruption of Mount Spurr by McNutt and Davis [2000]. In the following sections, we apply a detection algorithm to continuous acoustic data to produce a lightning catalog based on glitches for the entire Bogoslof eruption. We also present new observations of volcanic thunder not shown previously by Haney et al. [2018] and investigate the source of lightning-related signals measured on a moored hydrophone on the northeast slope of Bogoslof. Taken together, these observations give a more complete picture of electrical activity during the 2016-17 Bogoslof eruption and provide further insight into the imprint of volcanic lightning on geophysical data streams.

Such knowledge can be used in real-time monitoring of explosive volcanic eruptions worldwide, in order to detect the occurrence of volcanic lightning as early as possible.

2. Data and Methods

We focus primarily on acoustic data from a 4-element microphone array named OKIF on the eastern slope of Okmok Volcano (Figure 1). These data have also been analyzed and described by Fee et al. [2019, this issue], Lyons et al. [2019, this issue], and Schwaiger et al. [2019, this issue]. Here, the 4 individual elements are referred to as OK01, OK02, OK03, and OK04. The sensors comprising the array are Chaparral 25Vx microphones sampled in time at 100 Hz. This sample rate means that both infrasound (< 20 Hz) and audible acoustic (>20 Hz) signals are recorded. At the time of the eruption, each sensor was connected to a wind reduction system consisting of a series of porous hoses [Petersen et al., 2006]. The digitizer is located near the central node (OK04) and the other 3 elements (OK01, OK02, and OK03) are connected to the digitizer via cabling set beneath thick vegetation, but not buried in soil. The array has an aperture of approximately 100 m and has a triangular shape with one of the array elements at the center (OK04). In addition to the Okmok microphone array, we also analyze data from a moored hydrophone located 7 km to the northeast of Bogoslof (Figure 1). The hydrophone instrumentation is similar to the deployment described by Bohnenstiehl et al. [2013].

At a range of 60 km from the volcano, the 4-element Okmok array is the closest microphone array in the AVO network to Bogoslof. In fact, the data from the Bogoslof eruption at the Okmok array are among the closest microphone array recordings of any volcanic eruption in Alaska. Only the array located at frequently-active Cleveland volcano in Alaska has captured explosive activity at closer range (15 km). Thus, although the wind and temperature structure of the atmosphere can strongly affect sound propagation over the 60 km range from the Okmok array to Bogoslof [Schwaiger et al., 2019a; Iezzi et al., 2019; Schwaiger et al., 2019b], the recordings give a rare opportunity in Alaska to make detailed array measurements of an acoustic eruption wavefield.

We process the acoustic waves measured on the Okmok array using least-squares beamforming [Olson and Szuberla, 2005]. In this method, we cross-correlate all possible pairs of acoustic elements and find the time-delay corresponding to the maximum value of normalized cross-correlation. When the normalized cross-correlation exceeds a certain value (e.g., 0.5), we accept the time-delay measurement as being of high quality. If enough delay times meet this criterion to uniquely determine a slowness vector, we form a vector of the delay times and linearly relate them to apparent slowness across the array:

$$\overrightarrow{\Delta t} = G\vec{s} = G[s_{NS}, s_{EW}]^T \quad (1)$$

where s_{NS} and s_{EW} are the values of apparent slowness in the north-south and east-west directions, respectively, and G is a matrix of apparent distances [Haney et al., 2018]. For the 4-element Okmok array, as many as 6 delay time measurements could contribute to the lefthand side of equation (1). Thus, G could be as large as a 6-by-2 matrix. To find the apparent slowness across the array, we multiply both sides of equation (1) by the transpose of G and solve the equation in the least-squares sense. Once s_{NS} and s_{EW} have been obtained, we find the trace velocity across the array using

$$v = 1/\sqrt{s_{NS}^2 + s_{EW}^2} \tag{2}$$

and the backazimuth θ with

$$\theta = tan^{-1}(s_{EW}/s_{NS}) \tag{3}$$

where error estimates can also be found on these parameters [Szuberla and Olson, 2004]. An additional consideration for beamforming is choice of frequency band. Previously, Haney et al. [2018] beamformed acoustic data in the 4-8 Hz band to detect volcanic thunder. Such a choice was a tradeoff between higher frequencies with better signal-to-noise for thunder versus the use of lower frequencies for which good coherence can be maintained across the microphone array. In the Results section, we show beamforming over several frequency bands to illustrate which parts of the spectrum are dominated by the eruptive source versus volcanic thunder.

In addition to beamforming, we also process the microphone array data with a multichannel short-term average/long-term average (STA/LTA) filter to detect broadband electromagnetic pulses, or glitches, induced by lightning. Such glitches have been recently measured by Anderson et al. [2018] during an eruption of Tungurahua Volcano in Ecuador. The electromagnetic pulse associated with a lightning stroke generates a strong disturbance in the electric potential field that propagates outward at the speed of light. This is the same disturbance measured directly by sensors in global lightning location networks, either operated by Vaisala [Said et al., 2010] or the World Wide Lightning Location Network or WWLLN [Hutchins et al., 2012]. The propagating disturbance can in turn interfere with geophysical equipment such as cabling, leaving a characteristic imprint on the data stream. For comparison to lightning data, we utilize both WWLLN and Vaisala catalogs for the Bogoslof eruption in our analysis. Both catalogs provide location and origin times of detected strokes, with the Vaisala catalog additionally giving measurement of peak current of the stroke.

We detect glitches on the Okmok microphone array by applying a short-term-average/long-term-average (STA/LTA) filter to the envelope of the acoustic data in the 35-45 Hz band. We choose this frequency band since it is where the glitches have the highest signal-to-noise ratio (SNR), with other forms of acoustic signals (e.g., background noise, Bogoslof events) being diminished in this band. Since the Okmok data are sampled at 100 Hz, we are only able to analyze the glitches up to 50 Hz; it is possible the glitches have even better SNR in higher frequency bands. Wind noise is a persistent problem in all frequency bands and, when it is present, detections of the glitches are hindered. For the length of the STA and LTA time windows, testing on individual glitches has shown that 0.5 sec and 2.5 sec, respectively, yield accurate timing since the duration of the glitches is on the order of 1 sec or less. A trigger is declared when the STA/LTA ratio exceeds a particular value for 3 of the 4 elements of the Okmok microphone array, and when there has been no trigger for 1 s previously. In a subsequent quality control step, we also require that trigger have a maximum over a time window from 2 seconds before the trigger to 4 seconds after that occurs within +/-0.4 sec of the trigger time. These last steps result in triggers that are relatively well-recorded and isolated from other triggers. However, there is the possibility that multiple glitches closely spaced in time are filtered out.

3. Results

Before discussing volcanic lightning catalogs derived from electromagnetic glitches, we first describe a new observation of volcanic thunder from the Bogoslof eruption that was not discussed in Haney et al. [2018]. This constitutes the third documented instance of volcanic thunder during the Bogoslof eruption, the others occurring on March 8 and June 10, 2017 [Haney et al., 2018]. We focus on the eruptive event of May 17, 2017 (Event 39), which was the first activity at Bogoslof following a 2-month-long hiatus. The main portion of the event lasted for over an hour and was clearly recorded on the Okmok microphone array. In Figure 2, we plot several parameters from this event derived from acoustic and lightning data. Panels A though C of Figure 2 show detections from least-squares beamforming in 3 non-overlapping frequency bands: 1-2 Hz, 2-4 Hz, and 4-8 Hz. We plot backazimuth of the detection from the array, with a backazimuth of 0° pointed toward the volcano. Negative backazimuths correspond to locations to the west of Bogoslof, and positive backazimuths indicate eastward locations. Backazimuths of lightning locations from the Vaisala catalog, relative to the Okmok array, are shown in panel D of Figure 2. To simplify the plot, we've only shown backazimuths for lightning strokes with absolute values of peak current greater than 5 kA. We do so in light of the results of Haney et al. [2018], which suggested volcanic thunder should only be measurable at the Okmok array for lightning strokes exceeding that peak current value. Strokes with smaller peak current are not expected to produce measurable volcanic thunder at 60 km range, since lightning peak current has been shown to scale with acoustic power [Assink et al., 2008]. The yellow shaded time periods in panels A-D are from Wech et al. [2018] and indicate when the volcano was inferred to be actively erupting. Finally, panel E of Figure 2 is a spectrogram of the acoustic data from the central element of the array (OK04).

As seen in Figure 2, the different frequency bands are sensitive to sources with varying backazimuths over the course of the eruptive event. We conclude from panel A that the lowest frequency band from 1-2 Hz is dominated by the volcanic eruption process related to mass ejection at the vent. The time of detections in panel A match closely with the eruption times shaded in yellow from Wech et al. [2018]. In fact, the existence of coherent low frequency infrasound from Bogoslof was the basis for the interpretation of eruption activity by Wech et al. [2018]. Panel B shows that the 2-4 Hz band is sensitive to the same eruptive process as in panel A; however, it is also sensitive to another phenomenon which continues in the 2 time periods after the volcano stops erupting (marked with red arrows in Figure 2). We interpret this pattern as being due to volcanic thunder continuing in the eruption plume after activity has ceased. We base this partly on the patterns observed by Haney et al. [2018], but also on the fact that the backazimuths systematically shift toward the west as indicated by the red arrows. The shift to the west agrees with the backazimuths of lightning strokes relative to the Okmok array in panel D. In particular, note that by 8:00 UTC the backazimuths in panels B and D have both deviated from the direction of the volcano by 30°, clearly indicating the signals are not being produced at the volcanic vent. This is a much larger backazimuth deviation than observed for the June 10 event by Haney et al. [2018], which was on the order of 3°. The time moveout of the red arrows in panel B are approximately 2 degrees per minute, which corresponds to a speed of ~10 m/s for a source at 60 km range. Panel C shows that in the 4-8 Hz band, volcanic thunder dominates over eruption infrasound, since the same backazimuth patterns for thunder are present as in Panel B. Especially interesting is that the 4-8 Hz detections begin at a time coincident with the onset of lightning detections. This suggests that the primary source of infrasound in this frequency range for Event 39 was from volcanic thunder. Note that such frequency partitioning is not necessarily the same for each eruptive event. As shown by Haney et al. [2018], the June 10, 2017 eruptive event generated significant infrasound in the 4-8 Hz band prior to the onset of lightning due to the eruptive process. The May 17 eruptive event had overall lower frequency content than the June 10 eruption, enabling volcanic thunder to be even more visible in the 4-8 Hz band.

In Figure 3, we plot spectrograms of the 4 elements of the microphone array during the 15-20 minutes following the cessation of eruptive activity on May 17. This is the time period when the backazimuths of acoustic detections dramatically shifted to the west. The diffuse signals between 0-20 Hz during the time period from 7:55-8:00 UTC are excellent examples of individual volcanic thunder claps. However, there are impulsive broadband signals during this time period, three of which are indicated by arrows in Figure 3. We interpret these as the electromagnetic pulses, or glitches, due to volcanic lightning strokes, similar to the ones reported by Anderson et al. [2018]. Prior to 7:55 UTC in Figure 3, there are a multitude of these glitches and they only become easily individually identifiable in the plot after 7:55 UTC. A couple basic properties of the glitches are apparent in Figure 3.

First, although the glitches are broadband, they have a particularly high signal-to-noise ratio in the 35-45 Hz band. In this high frequency band, other signals are comparatively absent. Secondly, the glitches show up most clearly on element OK01, less clearly on elements OK02 and OK03, and are not even discernable on element OK04.

This pattern of relative amplitudes among the 4 elements of the array was observed for glitches throughout the Bogoslof eruption and has a simple explanation based on the geometry of the Okmok microphone array, as shown in Figure 4. Volcanic lightning mostly occurred to the north of the array, in the vicinity of Bogoslof [Van Eaton et al., this issue]. The northerly origin of the lightning maximizes the apparent distance of the cable run from the digitizer (closely located to central element OK04) to OK01 in the direction of the lightning. The longer apparent distance from OK01-OK04 translates into a larger voltage drop across the ends of the cable, induced by the electromagnetic pulse of the lightning, than the voltages induced on the shorter apparent distances of the OK02-OK04 and OK03-OK04 cable runs. Since OK04 is itself virtually co-located with the digitizer, negligible voltage is induced. From the geometry of the array, we can estimate that the induced voltage on element OK01 should be approximately twice the induced voltages on OK02 and OK03. Shown in the inset of Figure 4 is an example of a single electromagnetic glitch on all four elements during the June 10, 2017 eruption. Indeed, in agreement with the estimate, the amplitude of the glitch on OK01 is about two times larger than on OK02 and OK03. No glitch is evident on element OK04. These patterns suggest a controlling factor of the glitch amplitude was the projection of the cable run in the direction of the lightning stroke, an idea also invoked by McNutt and Davis [2000] to explain glitches in seismic data during the 1992 eruption of Mount Spurr.

Here we exploit the occurrence and pattern of glitches for the bulk processing of the 4 Okmok array elements over the entire 8-month-long Bogoslof eruption sequence, with the goal of defining a lightning catalog for Bogoslof based on glitches. To detect the glitches, we use the STA/LTA approach discussed previously and widely used in producing event triggers and automatically picking first breaks in seismic data processing. We apply the algorithm to envelopes of 35-45 Hz bandpassed acoustic data on the Okmok array. We have computed 2 different catalogs: one requiring an STA/LTA ratio of 2.8 to trigger, called Glitch Catalog A, and the other using a lower value of 2.3 for the ratio, called Glitch Catalog B. The value of 2.3 is the same as used in standard real-time processing of seismic data at AVO [Dixon et al., 2012] and will generally yield more detections than the value of 2.8. A detail is that the STA/LTA algorithm we employ also requires a quiet time before a trigger (1 second), and so in some rare cases the use of a lower STA/LTA triggering ratio can result in a new trigger being generated immediately before a trigger obtained with a higher ratio, thereby arresting the later trigger. However, in general, lower values of STA/LTA ratio result in more triggers. The tradeoff in the two catalogs is that Glitch Catalog A, which uses the ratio of 2.8, has fewer false detections. Glitch Catalog B, with a ratio of 2.3, detects more glitches and is preferable for retrospective data analysis, but results in more false detections (i.e., false alarms). Thus, the STA/LTA ratio used in Glitch Catalog A would likely be better suited for real-time implementation, when false alarms are a greater concern. We discuss and analyze both catalogs in the remainder of this section.

The application of the STA/LTA detector over the entire Bogoslof eruption results in 514 triggers for Glitch Catalog A and 1309 triggers for Glitch Catalog B. Of the 514 and 1309 raw triggers for the two catalogs, 399 and 814 triggers, respectively, occur during time periods of volcanic lightning already known from the existing WWLLN and Vaisala catalogs. As a result, we conclude these are true detections. We define these time windows for each of the 31 Bogoslof events with WWLLN or Vaisala lightning based on the first and the last strokes from the combined WWLLN/Vaisala catalog. However, for Glitch Catalog A, we have examined the raw triggers that occurred outside of these time windows and find that 23 of the remaining 115(=514-399) triggers are in fact new volcanic lightning strokes not represented in the WWLLN/Vaisala catalogs. For Glitch Catalog B, we find that 48 of the remaining 451(=1309-814) triggers are new volcanic lightning strokes. We discuss some of these new strokes later in this section. In fact, 4 of the new strokes occurred during an eruptive event for which no strokes were previously known to exist in the WWLLN or Vaisala catalogs (Event 56 on July 2, 2017). Thus, Glitch Catalog A finally consists of 422 total volcanic lightning strokes (422/518 or 81% detection success rate), and Glitch Catalog B consists of 862 (862/1309 or 66% detection success rate). Table 1 gives a summary of the number of detections for both catalogs over all Bogoslof events with glitches.

The remaining glitch triggers are false detections insofar as we cannot unequivocally associate them with instances of volcanic lightning. Many of them are related to meteorological lightning that occurred over the course of the 8-month-long eruption. Meteorological lightning is rare in the Aleutian Islands compared to other regions;

however, a significant meteorological lightning storm occurred in the Aleutians on July 16 and 17, 2017 and contributed many of the false detections. A small amount of meteorological lightning occurred at a low background rate throughout the 8 months as well. We hold off on addressing the possibility of filtering out these detections of meteorological lightning for future work.

In Figure 5, we plot envelopes all 422 glitch detections comprising Glitch Catalog A in a 6 second time window around the glitch (2 seconds pre-trigger and 4 seconds post-trigger). By taking the mean over all the glitches, we obtain the average envelopes shown in Figure 6. The average envelopes bear out the relative amplitude pattern discussed previously; namely, that glitches on element OK01 are on average larger than OK02 and OK03, and that glitches barely exist on OK04. Note that the amplitude on element OK02 is slightly larger than OK03 in Figure 6. This may be due to the average backazimuth of volcanic lighting over the entire eruption coming from the direction of Bogoslof, which is roughly 8 degrees west of north. The overall preference for incident azimuths coming slightly from the west increases the apparent distance along the OK02 cable run relative to OK03, thereby increasing the average glitch amplitude. Also note that the glitch amplitude on OK01, being close to 200 counts, corresponds to an induced voltage of approximately 0.5 mV given the digital conversion of the Q330 digitizer at the Okmok array of 419430 counts/V. We note this value but do not currently have a model to explain the coupling of the propagating electromagnetic wave from the lightning stroke with the induced voltage.

Shown in Figure 7 are time histories of glitch peak amplitude for two of the Bogoslof events, using Glitch Catalog B. In panels A and B, glitch detections are plotted for the January 31, 2017 eruption (Event 29) and May 17, 2017 eruption (Event 39), respectively. The yellow shaded areas are the time windows determined from the first and last volcanic lightning strokes in the combined WWLLN/Vaisala catalog. Several new strokes are detected before the WWLLN/Vaisala time window for the May 17 event. No such early strokes are found for the January 31 event; however, the glitch catalog includes several strokes prior to 8:00 UTC which were not detected by WWLLN.

Given the detection times in Glitch Catalog A and Glitch Catalog B, we have attempted to associate the glitches with individual strokes in the Vaisala catalog. To do so, we find the closest origin time of a Vaisala stroke to a glitch detection and associate them if they are within 1 second of each other. In this fashion, 286 of the 422 detections in Glitch Catalog A can be associated with individual Vaisala strokes. Similarly, 528 of the 862 detections in Glitch Catalog B can be associated. In Figure 8A, we have plotted the time difference between the Vaisala origin time and the glitch detection time for the associated strokes in Glitch Catalog B. On average, the difference is observed to be a small time delay on the order 0.1 seconds. We interpret this time delay as due to the time it takes for the STA/LTA filter to be activated once encountering a glitch. In Figure 8B, we show normalized histograms of Vaisala-computed peak currents for the Vaisala strokes associated with Glitch Catalogs A and B, as well as for all the Vaisala strokes. The associated strokes are observed to be enriched in higher peak currents, suggesting that the glitches tend to be from strokes with higher peak current. This dependence is further explored in Figure 9, which shows linear regressions on a log-log plot between glitch amplitude on all 4 array elements and peak current for the associated strokes in Glitch Catalog A. The regressions show a weak dependence between glitch amplitude and peak current for elements OK01, OK02, and OK03, although the scatter means other factors must play a role in determining the glitch amplitude as well.

We show details of previously unknown volcanic lightning strokes in Figures 10 and 11 for the June 10 and July 2, 2017 eruptions. Panel A of Figure 10 depicts a known volcanic lightning stroke that occurred at approximately 13:12 UTC on June 10. Volcanic thunder arrives about 3 minutes later due to the 60 km range from Bogoslof, shortly after 13:15 UTC. Note that the signal prior to the glitch in Figure 10A is volcanic thunder from an earlier stroke not shown in the plot. In panels B, C, and D of Figure 10, we show new strokes found from glitch detections at 11:14, 11:44, and 13:25 UTC. Each of these strokes is followed by volcanic thunder about 3 minutes later, further confirming that the glitches are produced by volcanic lightning. The 11:14 UTC stroke is particularly notable since it occurs over an hour before the first WWLLN or Vaisala stroke for this event. Data from lightning sensors in Dutch Harbor and Adak indicates the 11:14 UTC stroke was intra-cloud, not cloud-to-ground. Although both the 11:14 and 11:44 UTC strokes occurred before the strongest phase of the June 10 event, note that unrest for the event started at 9:58 UTC, over an hour before the 11:14 UTC stroke. Figure 11 shows 4 glitch detections for the July 2, 2017 eruption, an event for which there were no detected strokes by WWLLN or Vaisala. Infrasound propagation between Bogoslof and the Okmok array was poor for this event, so we also plot the Okmok seismic station OKER to illustrate the strongest portion of the eruptive event. Although the first detection appears to occur near the beginning of the event, Tepp and Haney [this issue] discuss the fact that subtle precursors had been ongoing for about an hour before the first glitch detection.

In Figures 12 and 13, we give details of signals observed on the hydrophone at Bogoslof (Figure 1) that coincide with volcanic lightning strokes during the June 10, 2017 eruptive event. Figure 12 shows a high frequency (50-300 Hz) hydroacoustic signal associated with the new stroke detected in the glitch catalogs at 11:14 UTC. The signal is clearly associated with the lightning stroke since no other similar signals are observed during the half-hour around the time of 11:14 UTC. Previously, hydroacoustic signals associated with lightning have been reported in the Gulf of Mexico [Arnold et al., 1984; Hill, 1985] and interpreted as due to lightning striking the ocean surface. We find an alternative explanation for the lightning-related hydroacoustic signals at Bogoslof: that the sound wave from thunder generated in the atmosphere undergoes acoustic reflection/transmission at the air-ocean interface and then propagates to the hydrophone. We base this inference on a few observations. The first is that the hydroacoustic wave is typically delayed by approximately 10 seconds relative to the electromagnetic glitch on the Okmok array, as shown in Figure 13 for the stroke at 13:12 UTC on June 10, 2017. A delay of 10 seconds, if the hydroacoustic wave is excited by a lightning strike to the ocean surface, would correspond to a travel distance of 15 km in the ocean. Taking into account the WWLLN and Vaisala lightning locations, which consistently place the 13:12 UTC stroke to the northeast of the volcano and close to the hydrophone, the distance (15 km) corresponding to a 10 s delay is too far from the hydrophone to correspond to a lightning strike on the ocean surface.

Secondly, as mentioned previously, data from a lightning sensors in Dutch Harbor and Adak indicate that the 11:14 UTC stroke was intra-cloud, not cloud-to-ground. Therefore, the hypothesis of a lightning strike to the ocean surface does not apply to the 11:14 UTC stroke, which clearly produced a signal associated with lightning (Figure 12). Finally, it is worth noting that the transmission coefficient of a pressure wave passing from air into water at normal incidence is 2 [Brekhovskikh, 1980; p. 11]. Thus, a pressure wave is in fact amplified during acoustic transmission from air into water. This is in contrast to the transmission coefficient from water into air, which is close to zero at normal incidence.

Given these considerations, our preferred interpretation of the hydroacoustic signals is that they are simply underwater recordings of high frequency volcanic thunder in the near source region. The 10 second delay time can be explained by the thunder source being distributed at an altitude of a few kilometers. Additional delay on the order of 1-2 seconds can then be accommodated by propagation within the ocean from the surface to the hydrophone, which was located at 231 m depth.

4. Discussion

The glitch-based catalogs we have developed have both advantages and disadvantages when compared to the WWLLN and Vaisala catalogs. Overall, the glitch catalogs, both A and B, have a similar detection rate as WWLLN. Simply in terms of the total number of detected volcanic lightning strokes during the eruption, WWLLN (670) falls in between Glitch Catalog A (422) and Glitch Catalog B (862). As seen in Table 1, many of the events with the largest number of strokes are similar between the catalogs. However, note that several eruptive events not displayed in Table 1 had WWLLN strokes but zero glitch detections and that those events tended to occur during the winter, in December 2016 and January 2017. For some of those events, telemetry for the Okmok microphone array was down and data were not received. However, there were several events without detected glitches in the winter even when the data were transmitted successfully. This leads to the observation that the glitch catalogs performed better during the summer while the global catalogs, both WWLLN and Vaisala, detected more strokes during the winter. One example of this is that the glitch catalogs detected strokes for the July 2, 2017 event (Figure 11) which went undetected by both WWLLN and Vaisala. We attribute this seasonal dependence to the higher level of storm and wind noise on the acoustic channels during the winter, which inhibits the STA/LTA detection. Future work is warranted on better glitch detector algorithms than the STA/LTA approach we have utilized in this study. Anderson et al. [2018] have suggested the use of a median filter, a type of nonlinear signal processing that can be used to both accentuate and suppress short-duration, impulsive signals.

Our detection of volcanic thunder for the May 17, 2017 eruption (Event 39) shown in Figure 2 brings the total number of Bogoslof events with documented volcanic thunder to three, including the previously reported observations for the March 8 (Event 37) and June 10 (Event 48) eruptions by Haney et al. [2018]. The time frame between March 8 and June 10 appears to have been optimal for volcanic thunder observations, reflecting a tradeoff between more lightning occurring in the winter and early spring [Van Eaton et al., this issue] versus better acoustic propagation and lower wind noise in the late spring into summer. A notable exception to this was Event 40 on May 28, 2017, which produced a sizable number of lightning detections in all the catalogs. However, lower level winds at Bogoslof during Event 40 were directed toward the northwest, away from Okmok, which hindered acoustic propagation.

Besides the Okmok microphone array, we have looked into whether glitches appeared on other regional microphone arrays and seismic stations. The two closest microphone arrays to Bogoslof, after the one at Okmok, are located near Cleveland and Akutan volcanoes. However, those arrays are sampled at a lower rate (50 Hz) than the Okmok array, which detracts from glitch detection and observations of high frequency thunder signals. It may also be that those arrays do not have good line-of-sight views of Bogoslof and the lower atmosphere above the volcano. In contrast, Bogoslof Volcano can be seen visually from the Okmok microphone array in clear viewing conditions. Regarding seismic data streams, we have detected glitches from the network located at Okmok, similar to the observations at Mt. Spurr by McNutt and Davis [2000]. However, the glitches appear mostly on analog short-period stations, which can have a complicated telemetry path prior to digitization. Thus whether the glitches are occurring at the seismic station or at its radio repeater isn't straightforward to establish. Moreover, the cabling details (e.g., cable orientation and length) are not known for the seismic stations as they are for the Okmok microphone array. This is on account of the array requiring such geometrical information to be known for array processing, in contrast to single seismic stations. In any case, a future investigation of glitches in seismic data streams is warranted despite these additional complexities.

5. Conclusion

We have investigated the signature of volcanic lightning in ground-based, geophysical data streams during the 2016-17 Bogoslof eruption. The eruption was a prolific producer of volcanic lightning over the course of its 8-month-long duration, and a microphone array located at 60 km range enabled the observation of volcanic thunder and electromagnetic pulses, or glitches, produced by volcanic lightning. We developed two new catalogs based on the properties of glitches and found several new strokes which went undetected by the WWLLN and Vaisala catalogs. We further investigated lightning-associated signals on a moored hydrophone located on the northeast slope of Bogoslof. Taken together, these observations give a more complete picture of electrical activity during the 2016-17 Bogoslof eruption. These findings should be helpful for diagnosing the occurrence of volcanic lightning in real-time, ground-based geophysical data streams during eruptions monitored by volcano observatories.

Table 1: Eruptive events with glitch-detected strokes compared to WWLLN catalog. Number of glitch-detected strokes are given for Glitch Catalog A along with the number from Glitch Catalog B in parenthesis.

Date of eruptive event	Glitch-detected strokes	WWLLN strokes
March 8, 2017 (Event 37)	100 (220)	200
May 17, 2017 (Event 39)	73 (135)	39
January 31, 2017 (Event 29)	49 (95)	54
August 7, 2017 (Event 63)	49 (89)	4
May 28, 2017 (Event 40)	39 (87)	66
February 17, 2017 (Event 33)	32 (62)	35
June 10, 2017 (Event 48)	25 (46)	7
December 22, 2016 (Event 7)	16 (34)	60
January 24, 2017 (Event 26)	13 (25)	13
January 27, 2017 (Event 28)	6 (10)	1
July 2, 2017 (Event 56)	4 (4)	0
January 15, 2017 (Event 20)	3 (5)	3
December 16, 2016 (Event 4)	2 (4)	6
January 4, 2017 (Event 15)	2 (13)	11
January 26, 2017 (Event 27)	2 (5)	7
February 20, 2017 (Event 36)	2 (5)	2
August 27, 2017 (Event 66)	2 (6)	0
January 9, 2017 (Event 17)	1 (7)	20
January 20, 2017 (Event 24)	1 (0)	1
June 13, 2017 (Event 49)	1 (2)	0
June 27, 2017 (Event 54)	0 (6)	2
February 18, 2017 (Event 35)	0 (2)	13

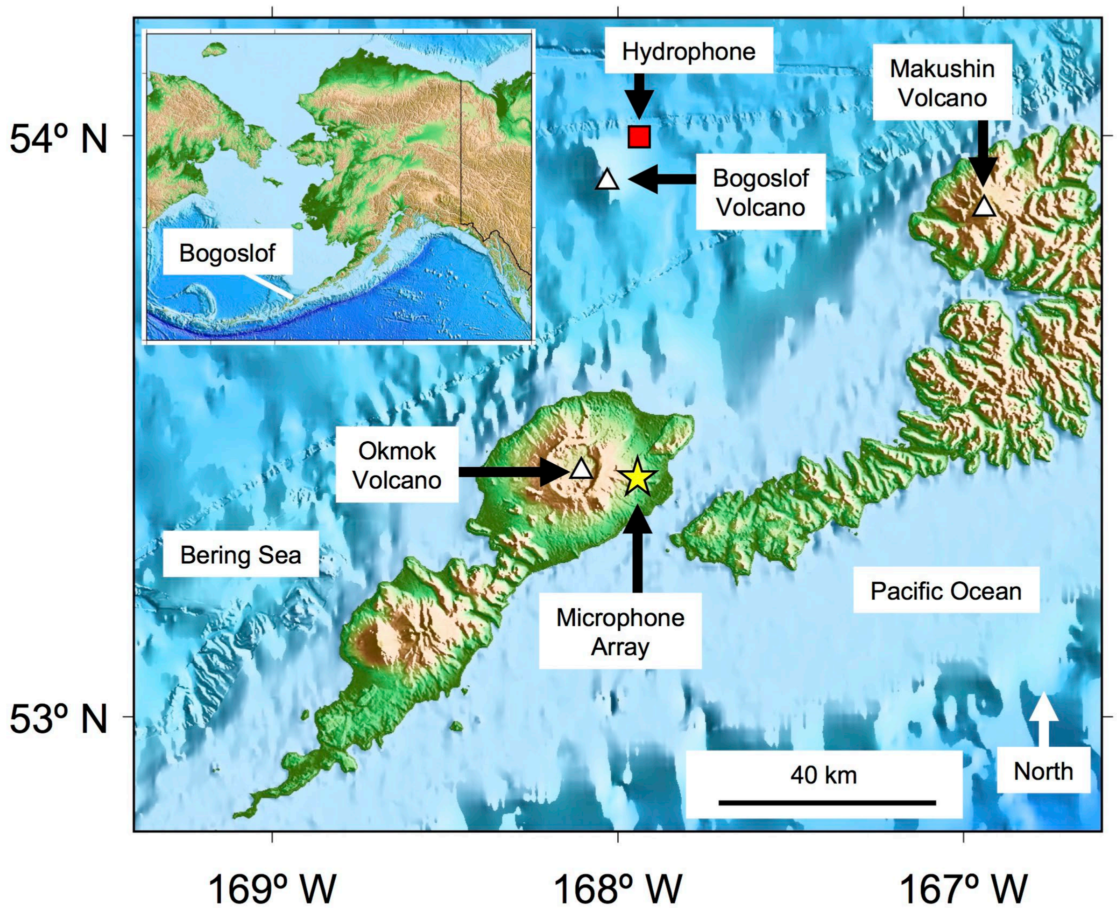

Figure 1: Regional map of Bogoslof Volcano and neighboring islands with inset showing the location of Bogoslof in the Alaska region. The microphone array located on the eastern slope of Okmok Volcano is indicated with a yellow star. A red square shows the location of a moored hydrophone 7 km northeast of Bogoslof.

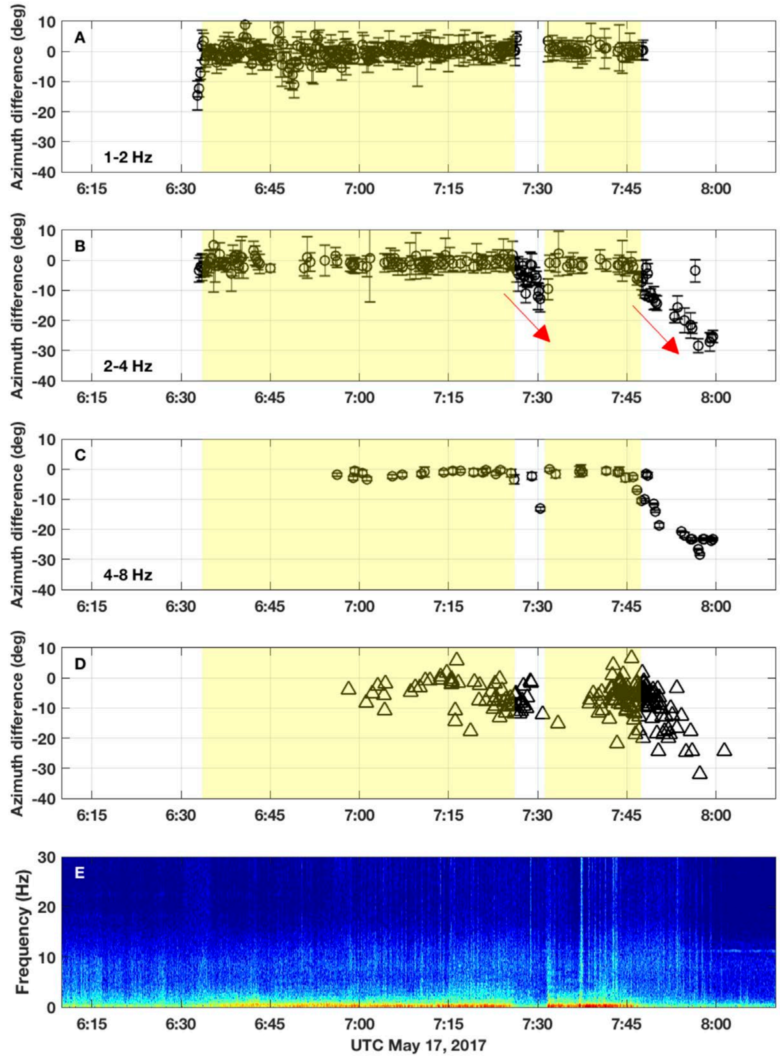

Figure 2: Measurements from the May 17, 2017 eruptive event, indicating the occurrence of volcanic thunder. Panels A-C depict backazimuths of detections on the Okmok microphone array in 1-2, 2-4, and 4-8 Hz bands. Panel D shows backazimuths relative to the Okmok microphone array of Vaisala lightning locations with peak current greater than 5 kA. In Panels A-D, a backazimuth of 0° points at Bogoslof. Yellow regions in panels A-D are times of eruptive activity from *Wech et al.* [2018]. Red arrows in Panel B show moveout of volcanic thunder signals. The lightning origin times are delayed by their Vaisala location assuming a nominal acoustic speed of 335 m/s. Panel E is a spectrogram of acoustic data from the central element of the array.

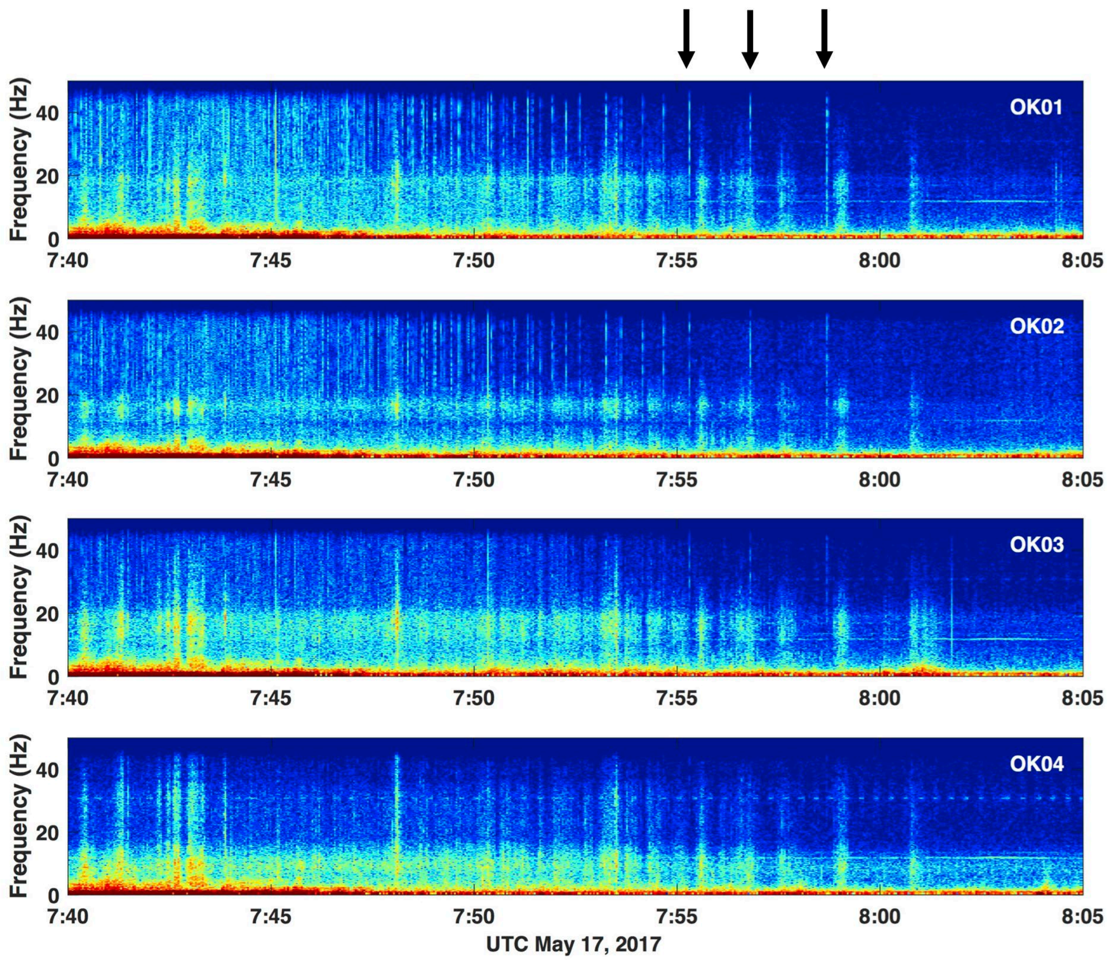

Figure 3: Waning portion of the May 17, 2017 eruptive event showing broadband glitches on elements 1-3 of the microphone array. The three final electromagnetic pulses from lightning, or glitches, are indicated with arrows.

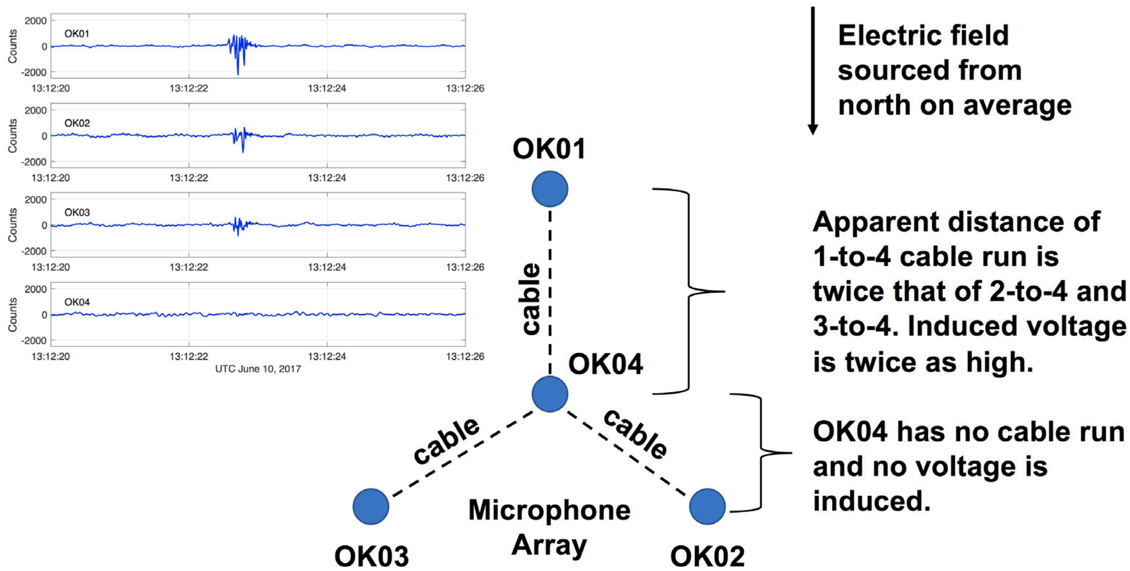

Figure 4: Schematic of the Okmok microphone array and representative glitch signal from eruptive event on June 10, 2017. Text within the figure provides a first-order explanation for the relative amplitudes of the glitches on the 4 elements of the microphone array.

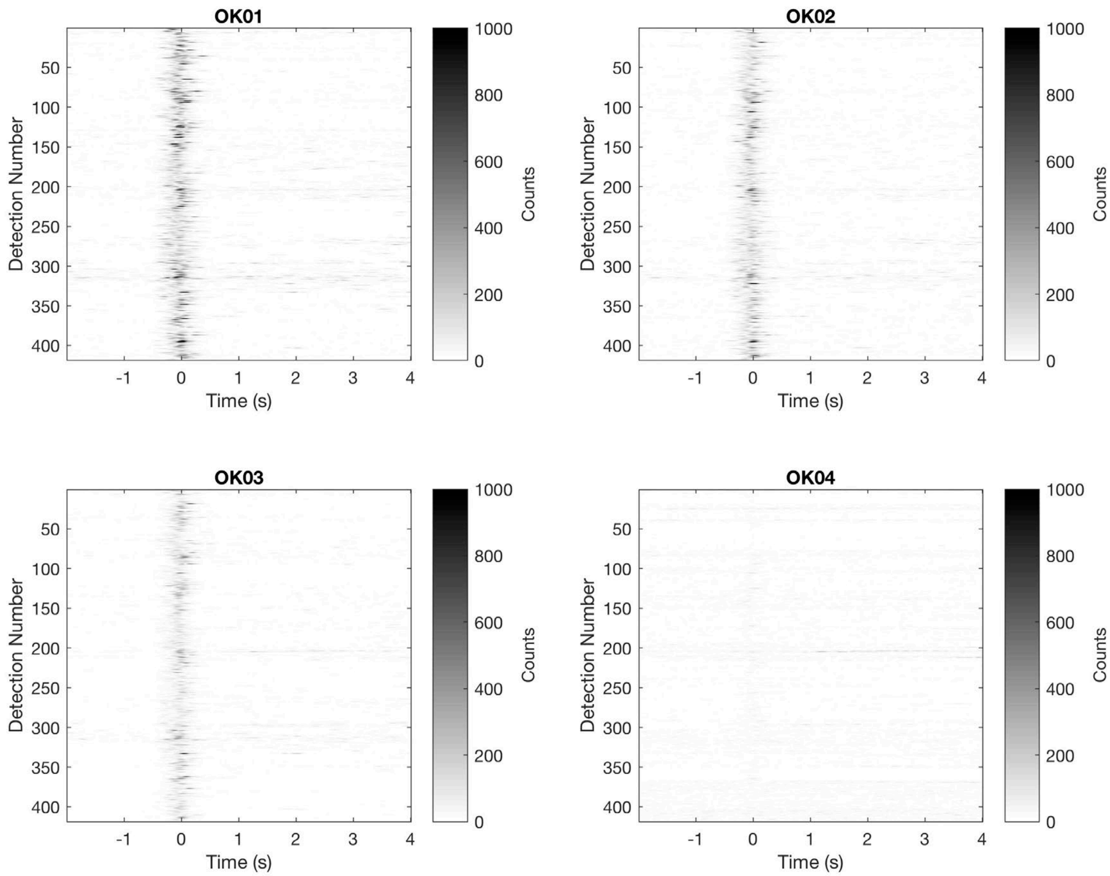

Figure 5: Glitch detections on the Okmok microphone array over a time period covering the entire eruption from December 1, 2016 to September 1, 2017. Envelopes of 35-45 Hz bandpassed acoustic data are plotted with time relative to the glitch envelope's peak. As seen in Figure 4, the glitches are strongest on element OK01 and virtually nonexistent on element OK04.

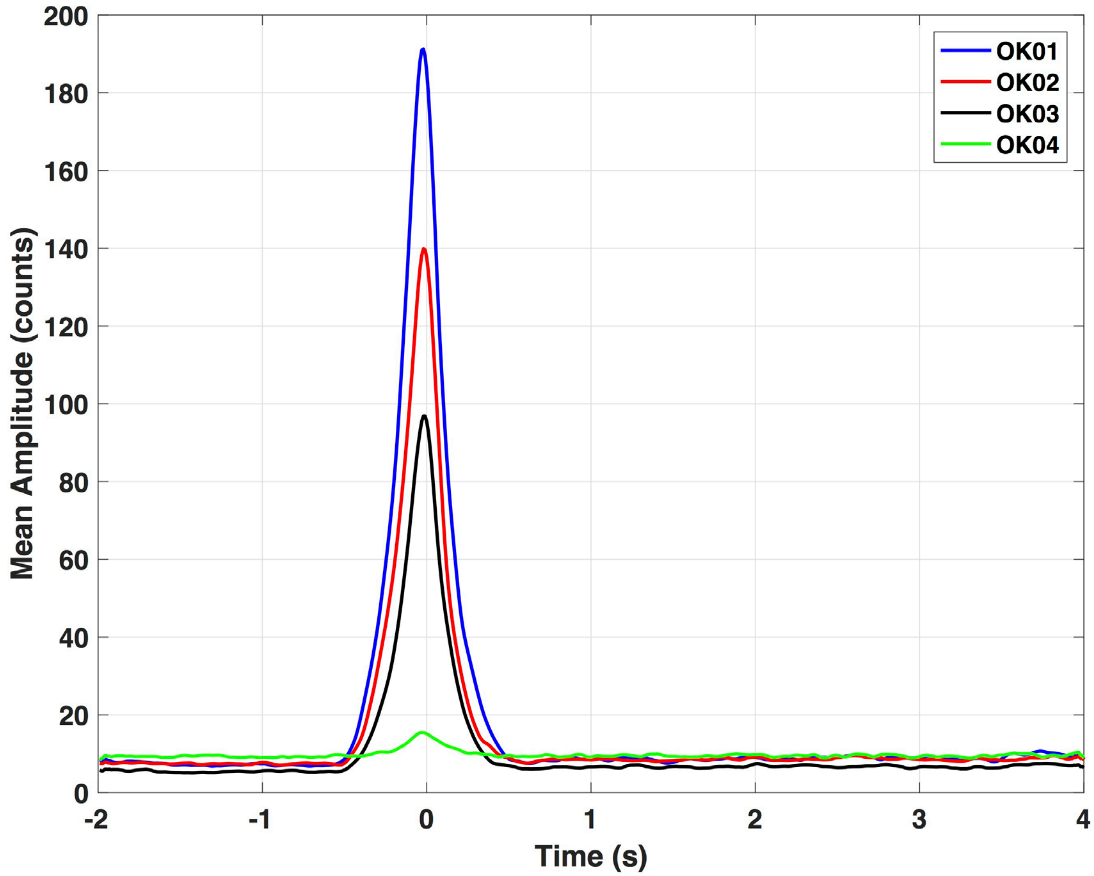

Figure 6: Average envelopes of the glitch detections shown in Fig. 5 for each of the 4 elements of the Okmok microphone array. The glitch envelope on OK01 is on average approximately twice as large as on OK02 and OK03.

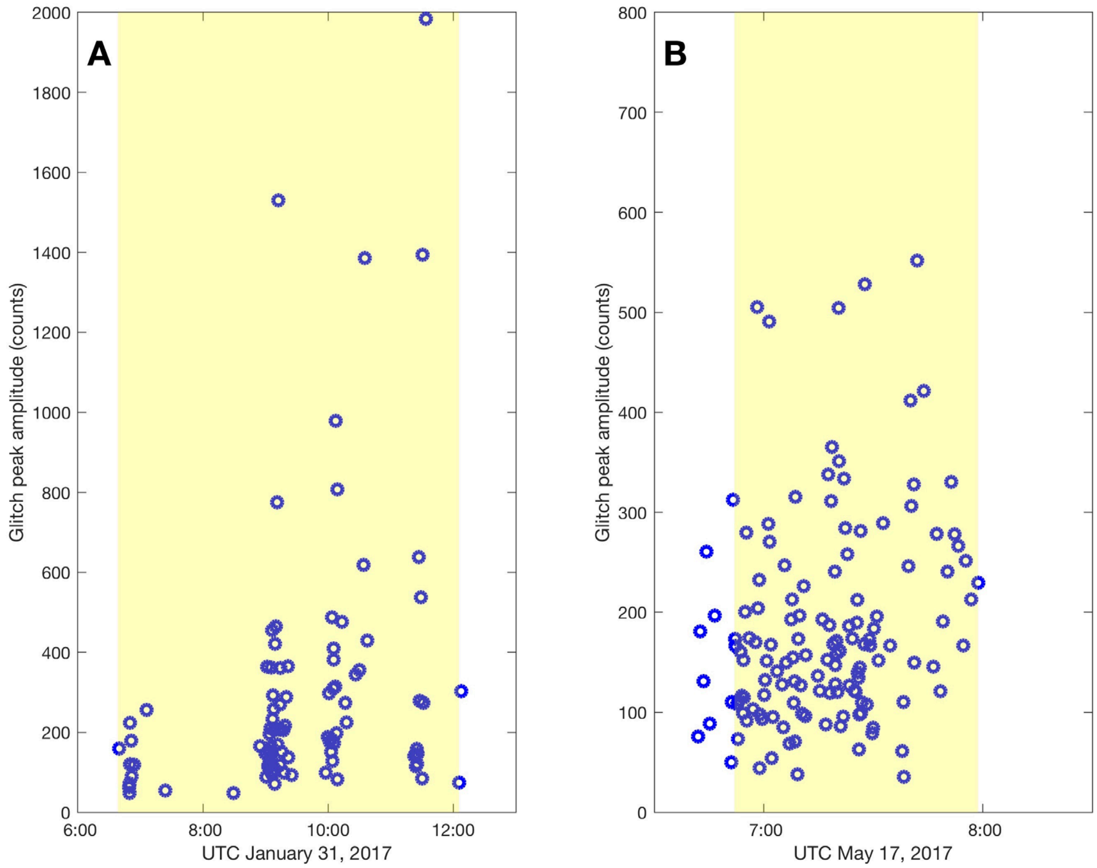

Figure 7: Peak amplitude of glitch detections versus time for two explosive eruptions of Bogoslof on January 31 (Event 29) and May 17 (Event 39), 2017. The glitch peak amplitude on OK01 is plotted on the y-axis, although panels A and B are at different scales. The time between the first and last stroke detected from a combined WWLLN/Vaisala catalog is shaded in yellow. Note that the glitches detected lightning prior to 8:00 UTC during Event 29, which were not detected by WWLLN. The glitches detected several strokes on May 17 in the minutes before the initial stroke in the combined WWLLN/Vaisala catalog.

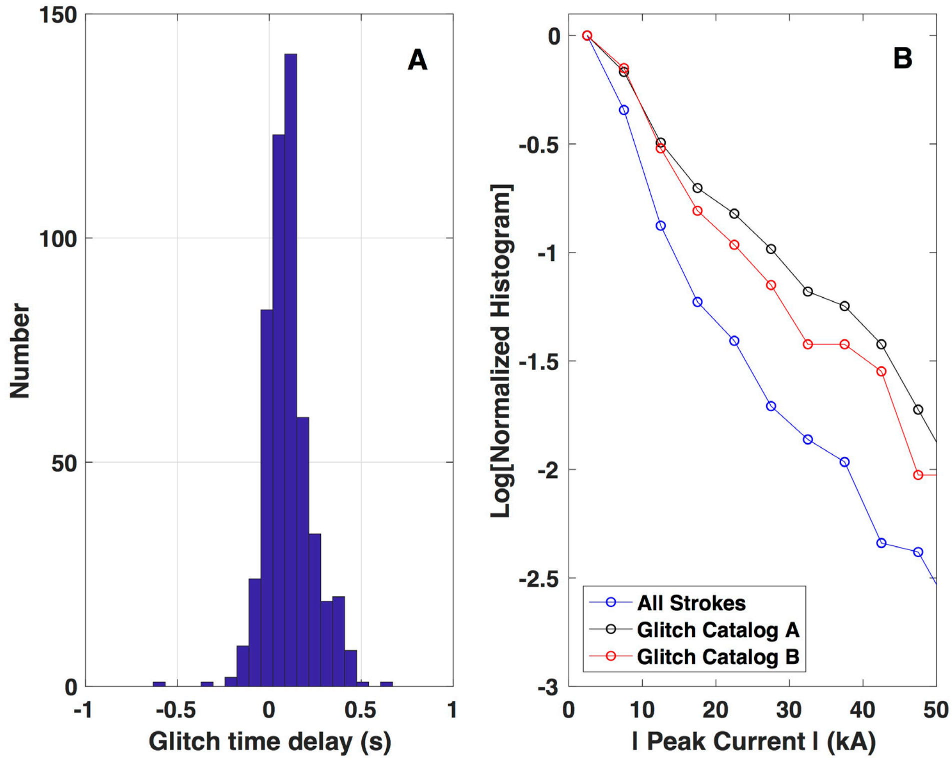

Figure 8: (A) Time delay between glitch detections and their association in the Vaisala catalog. The overall small, positive delay time is the result of the filtering action of the STA/LTA filter and shows the precision of the relative times between the glitches and the Vaisala catalog. (B) Logarithmic plot of normalized histograms versus peak current for the entire Vaisala catalog (blue), the subset of the catalog associated with Glitch Catalog A (black), and Glitch Catalog B (red). The normalized histogram from the glitch-associated strokes is seen to be enriched in higher peak current strokes compared to the entire catalog, suggesting that the strokes detected by the glitches are preferentially stronger than the ones that were not detected. This effect also explains why Glitch Catalog A is more enriched in higher peak current strokes than Glitch Catalog B.

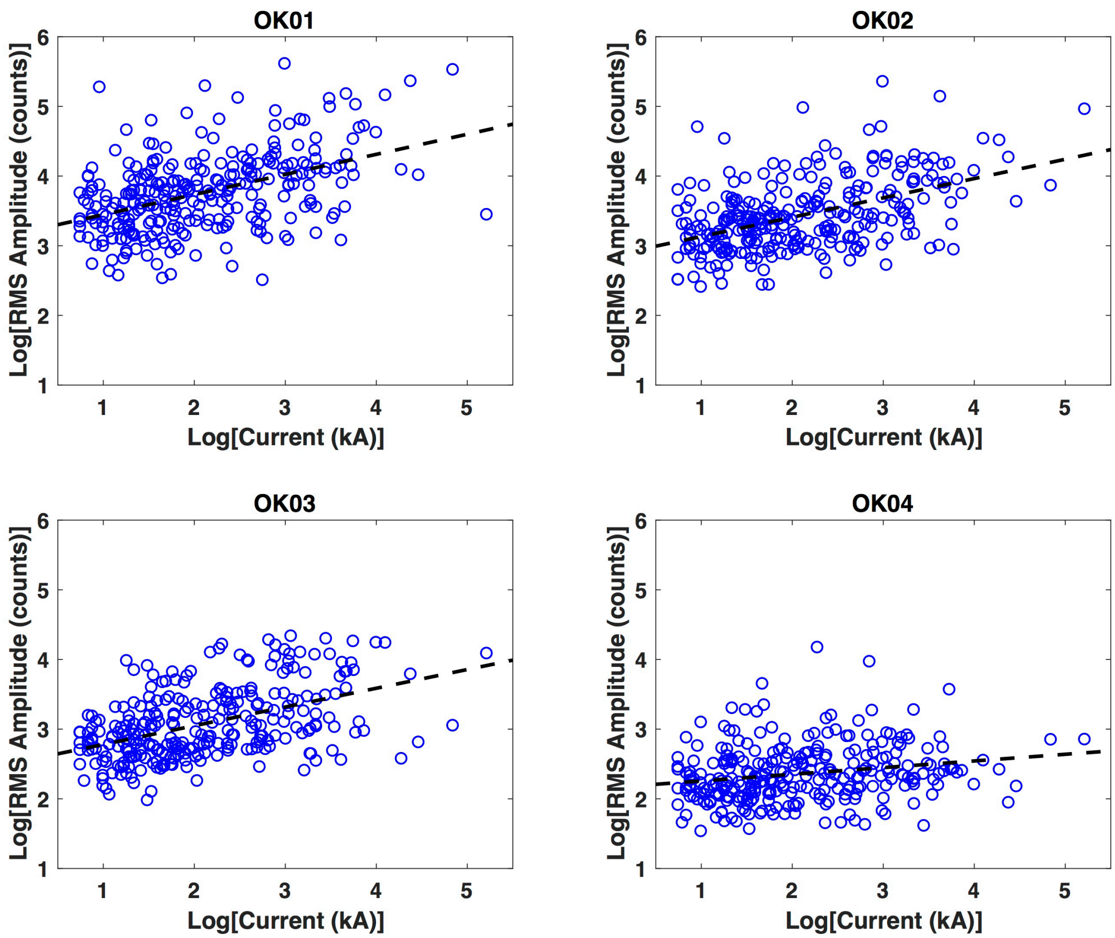

Figure 9: Logarithmic regression of the root-mean-square glitch amplitude versus the Vaisala peak current. A weak positive correlation exists on OK01, OK02, and OK03, with a power law exponent of approximately 0.25. Element OK04 has less, if any, dependence since it is not as susceptible to the voltages induced by the lightning discharge. This is further evidence, in addition to Figure 8B, that the strength of the lightning stroke has an general effect on the amplitude of the electromagnetic glitch, although other factors may exist.

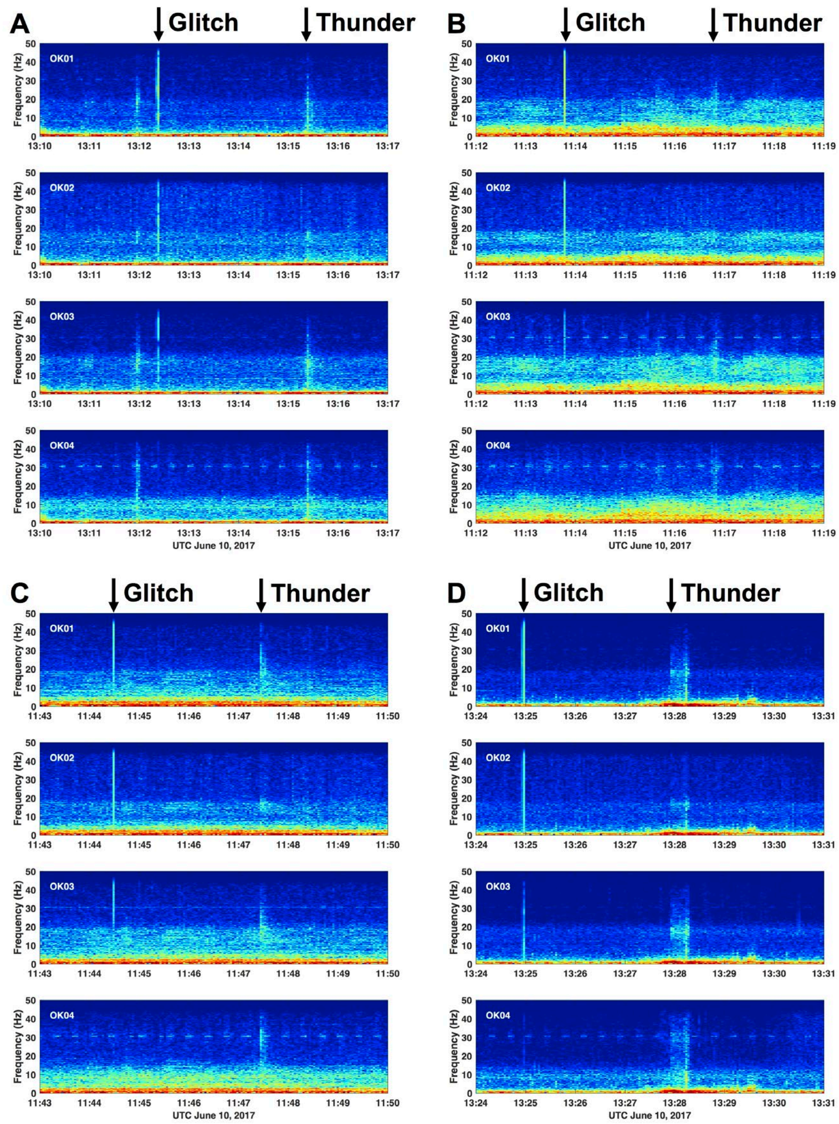

Figure 10: Examples of glitches and associated thunder signals during the June 10, 2017 eruptive event. Panel A shows a glitch from a known stroke in the WWLLN/Vaisala catalogs at approximately 13:12:15 UTC. Panels B-D show new strokes detected with glitches that do not exist in the WWLLN/Vaisala catalogs. In all panels, volcanic thunder is observed to arrive roughly 3 minutes after the glitch, further confirming the new detections in panels B-D. In panel A, volcanic thunder from a stroke prior to the time window arrives before the glitch.

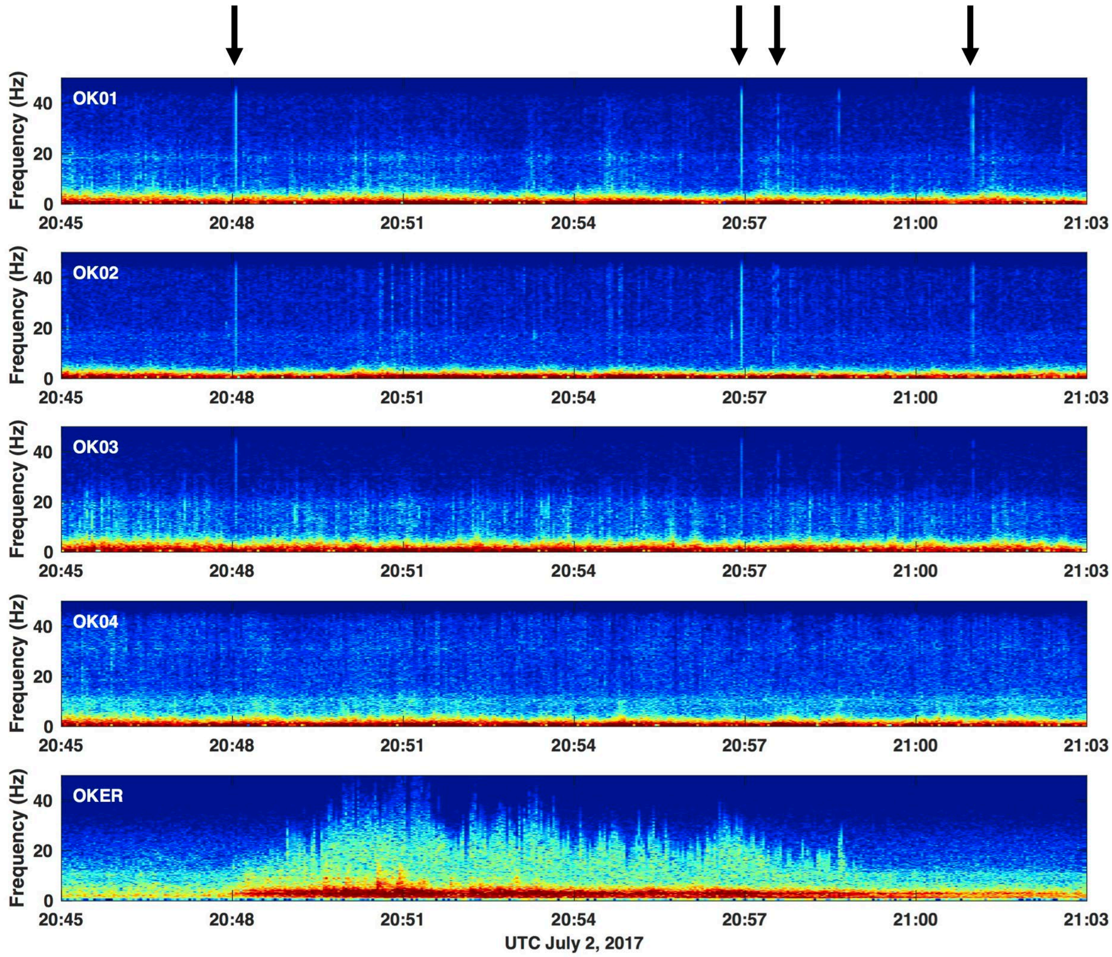

Figure 11: Volcanic lightning detected from glitches during the July 2, 2017 eruption (Event 56). These detections were noteworthy because no strokes exist for this event in the combined WWLLN/Vaisala catalog. Sound propagation from Bogoslof to the Okmok array was poor on July 2 and as a result no eruptive infrasound or volcanic thunder appears in the microphone array data. Okmok seismic station OKER is included at the bottom to indicate times of strong eruptive activity.

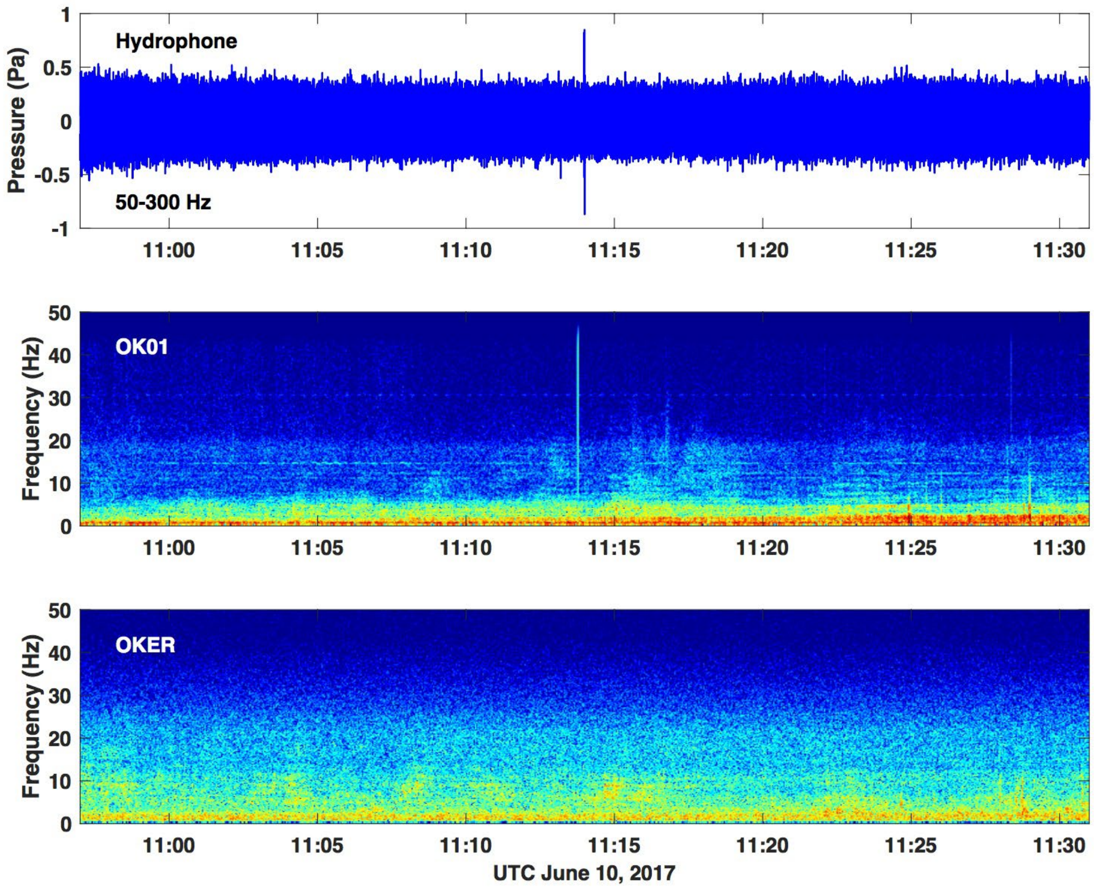

Figure 12: Hydroacoustic signal during the June 10, 2017 eruptive event associated with the lightning stroke at approximately 11:14 UTC. The hydroacoustic signal exists in the relatively high frequency band from 50-300 Hz and is clearly associated with the glitch (which it follows by 10 seconds) since no other high amplitude, impulsive hydroacoustic arrivals are observed during the 34-minute time window shown. Okmok seismic station OKER is also displayed to show that no short duration, impulsive signals existed in seismic data.

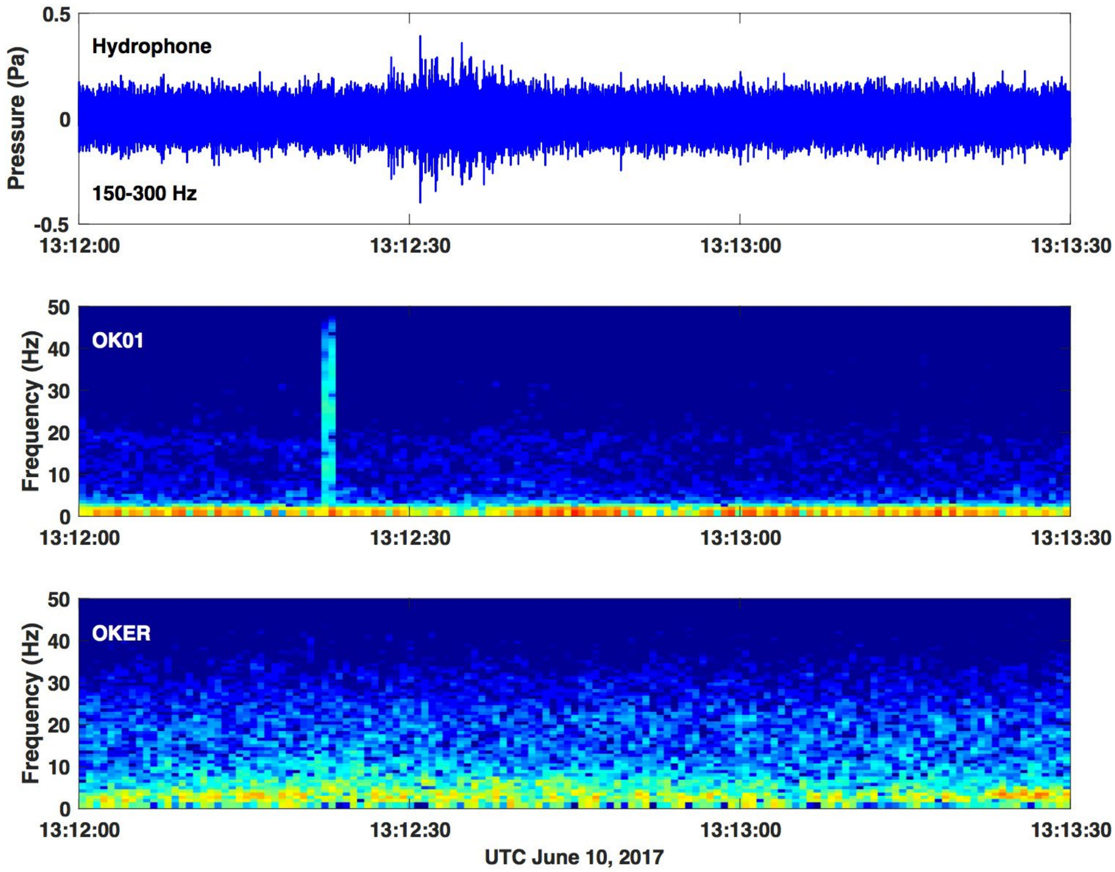

Figure 13: High-frequency (150-300 Hz) hydroacoustic signal following a volcanic lightning stroke during the June 10, 2017 eruption (Event 48). The hydroacoustic signal arrives approximately 10 s after the glitch. The glitch occurs within a second of the origin time of the associated stroke in the WWLLN/Vaisala catalogs. The 10 s time delay is too long to be explained by direct propagation in the water column from the lightning location to the hydrophone, and suggests the hydroacoustic signal originates as high frequency thunder that is acoustically transmitted from the atmosphere into the ocean.

References

Anderson, J. F., Johnson, J. B., Steele, A. L., Ruiz, M. C., and Brand, B. D. (2018). Diverse eruptive activity revealed by acoustic and electromagnetic observations of the 14 July 2013 intense Vulcanian eruption of Tungurahua volcano, Ecuador. *Geophys. Res. Lett*., 45, 2976-2985.

Arnold, R. T., Bass, H. E., and Atchley, A. A. (1984). Underwater sound from lightning strikes to water in the Gulf of Mexico. *J. Acoust. Soc. Am.*, 76(1), 320-322.

Assink, J. D., Evers, L. G., Holleman, I., and Paulssen, H. (2008). Characterization of infrasound from lightning. *Geophys. Res. Lett*., 35, L15802.

Behnke, S. A., and McNutt, S. R. (2014). Using lightning observations as a volcanic eruption monitoring tool. *Bull. Volcanol*., 76, 847. 10.1007/s00445-014-0847-1

Behnke, S. A., and Bruning, E. C. (2015). Changes to the turbulent kinematics of a volcanic plume inferred from lightning data. *Geophys. Res. Lett*., 42, 4232-4239.

Bohnenstiehl, D. R., Dziak, R. P., Matsumoto, H., and Lau, T.-K. A. (2013). Underwater acoustic records from the March 2009 eruption of Hunga Ha'apai-Hunga Tonga volcano in the Kingdom of Tonga. *J. Volcanol. Geotherm. Res*., 249, 12-24.

Brekhovskikh, L. M. (1980). Waves in Layered Media. New York: Academic Press.

Campus, P., and Christie, D. (2009). Worldwide observations of infrasonic waves. In A. Le Pichon, E. Blanc, & A. Hauchecorne (Eds.), Infrasound monitoring for atmospheric studies (pp. 185–234). Netherlands: Springer.

Coombs, M. L., Wech, A. G., Haney, M. M., Lyons, J. J., Schneider, D. J., Schwaiger, H. F., Wallace, K. L., Fee, D., Freymueller, J. T., Schaefer, J. R., and Tepp, G. (2018).

Short-term forecasting and detection of explosions during the 2016–2017 eruption of Bogoslof volcano, Alaska. *Frontiers in Earth Science*, 6, 122, 17 pp.

Coombs, M., Wallace, K., and Cameron, C. (2019). Overview, chronology, and impacts of the 2016-2017 eruption of Bogoslof volcano. *Bull. Volcanol*., this issue.

Dixon, J., Stihler, S., Power, J., Haney, M., Parker, T., Searcy, C., and Prejean, S. (2013). Catalog of earthquake hypocenters at Alaskan volcanoes: January 1 through December 31, 2012, U.S. Geol. Surv. Data Ser., 789, 84.

Fee, D., Lyons, J., Haney, M., Wech, A., Waythomas, C., Diefenbach, A., Lopez, T., Van Eaton, A., and Schneider, D. (2019) Seismo-acoustic evidence for vent drying during shallow submarine eruptions at Bogoslof volcano, Alaska. *Bull. Volcanol*., this issue.

Haney, M. M., Van Eaton, A. R., Lyons, J. J., Kramer, R. L., Fee, D., and Iezzi, A. M. (2018), Volcanic thunder from explosive eruptions at Bogoslof Volcano, Alaska, *Geophys. Res. Lett.,* 45, 3429-3435.

Hill, R. D. (1985), Investigation of lightning strikes to water surfaces, *J. Acoust. Soc. Am.*, 78(6), 2096-2099.

Hutchins, M. L., Holzworth, R. H., Rodger, C. J., & Brundell, J. B. (2012). Far-field power of lightning strokes as measured by the World Wide Lightning Location Network. *Journal of Atmospheric and Oceanic Technology*, 29, 1102–1110.

Iezzi, A. M., Schwaiger, H. F., Fee, D., and Haney, M. M. (2019). Application of an updated atmospheric model to explore volcano infrasound propagation and detection in Alaska. *J. Volcanol. Geotherm. Res.*, 371, 192-205.

Johnson, J. B., Arechiga, R. O., Thomas, R. J., Edens, H. E., Anderson, J., and Johnson, R. (2011). Imaging thunder. *Geophys. Res. Lett.*, 38, L19807.

Lyons, J., Fee, D., Haney, M., and Iezzi, A. (2019). Infrasound generated by the shallow submarine eruption of Bogoslof volcano, Alaska. *Bull. Volcanol*., this issue.

Mather, T. A. and R. G. Harrison (2006), Electrification of volcanic plumes, *Surv. Geophys.,* 27, 387-432.

McNutt, S. R. and C. M. Davis (2000), Lightning associated with the 1992 eruptions of Crater Peak, Mount Spurr Volcano, Alaska, *J. Volcanol. Geotherm. Res.*, 102, 45-65.

Olson, J. V., & Szuberla, C. A. L. (2005). Distribution of wave packet sizes in microbarom wave trains observed in Alaska. *The Journal of the Acoustical Society of America*, 117(3), 1032–1037.

Petersen, T., De Angelis, S., Tytgat, G., & McNutt, S. R. (2006). Local infrasound observations of large ash explosions at Augustine Volcano, Alaska, during January 11–28, 2006. *Geophysical Research Letters*, 33, L12303.

Said, R. K., Inan, U. S., & Cummins, K. L. (2010). Long-range lightning geolocation using a VLF radio atmospheric waveform bank. *Journal of Geophysical Research*, 115, D23108.

Schwaiger, H. F., Iezzi, A. M., and Fee, D. (2019a). AVO-G2S: A modified, open-source Ground-to-Space atmospheric specification for infrasound modeling. *Computers and Geosciences*, 125, 90-97.

Schwaiger, H., Lyons, J., Iezzi, A., Fee, D., and Haney, M. (2019b). Evolving infrasound detections from Bogoslof volcano, Alaska: insights from forward modelling. *Bull. Volcanol.,* this issue.

Szuberla, C. A. L., and Olson, J. V. (2004). Uncertainties associated with parameter estimation in atmospheric infrasound arrays. *The Journal of the Acoustical Society of America*, 115(1), 253–258.

Tepp, G. and Haney, M. (2019). Comparison of Short-term Seismic Precursors and Explosion Parameters during the 2016-2017 Bogoslof Eruption. *Bull. Volcanol*., this issue.

Thomas, R. J., Krehbiel, P. R., Rison, W., Aulich, G., Edens, H., McNutt, S. R., Tytgat, G., and Clark, E. (2007). Electrical activity during the 2006 Mount St. Augustine volcanic eruptions. *Science*, 315, 1097.

Van Eaton, A. R., Amigo, A., Bertin, D., Mastin, L. G., Giacosa, R. E., Gonzalez, J., et al. (2016). Volcanic lightning and plume behavior reveal evolving hazards during the April 2015 eruption of Calbuco volcano, Chile. *Geophysical Research Letters*, 43, 3563–3571.

Van Eaton, A., Schneider, D. J., Smith, C., Mastin, L., Haney, M., and Lyons, J. (2019). Overview of volcanic lightning at Bogoslof: detection, characteristics and seasonal effects. *Bull. Volcanol*., this issue.

Wech, A., Tepp, G., Lyons, J., and Haney, M. (2018). Using earthquakes, T Waves, and infrasound to investigate the eruption of Bogoslof volcano, Alaska. *Geophysical Research Letters*, 45. https://doi.org/10.1029/2018GL078457